# Verification of the Compton Wavelength and the Klein-Nishina Cross-Section

Bhaskar Mookerji and Charles Herder*
*MIT Department of Physics, 8.13*
(Dated: December 7, 2007)

We examine the angular and linear attenuation of gamma rays from a 100mCi $^{137}$Cs source Compton scattering off an NaI scintillation detector and three insulating plastics: polypropylene (PP), polyvinyl toluene (PVT), and polycarbonate (PC). From the Compton wavelength shift, we determine the mass of the electron as $510.9889 \pm 0.00044$keV and photon energy of a $^{137}$Cs source as $661.6 \pm 0.05$keV, each within $1\sigma$ of accepted values. The Klein-Nishina differential cross section for Compton scattering is confirmed, and the total electron cross section is measured to 0.25b.

The study of relativistic photon-matter interactions motivated early quantum theory and are a focus of modern quantum field theory. A subset of these—the photoelectric effect and Compton scattering—are commonly used to show that light (i) exhibits *wave-particle* dualism, and (ii) is either absorbed or scattered in a *quantized* manner when interacting with material particles [1].

Our goal here is to confirm the relativistic nature of Compton scattering in materials. We first describe the Compton wavelength shift of a single photon process and discuss the assumptions behind the Klein-Nishina formula describing its cross section. The mass of the electron is measured from the Compton wavelength, and Compton cross section is measured by characterizing the angular and mass attenuation of the Compton profile.

## 1. THEORY OF COMPTON SCATTERING

Our experiment focuses on single-photon Compton scattering, where an electron of momentum $p$, and a photon of momentum $k$ and polarization $e$, scatter into an electron of momentum $p'$, and a photon of momentum $k'$ and polarization $e'$[2]. The initial and final states of this process are shown in Figure 1. Applying energy and momentum conservation to the electron and photon 4-vectors $p_\mu$ and $k^\mu$, it can be shown that frequency $\omega$ of an incident photon scattered by an angle $\theta$ shifts to $\omega'$:

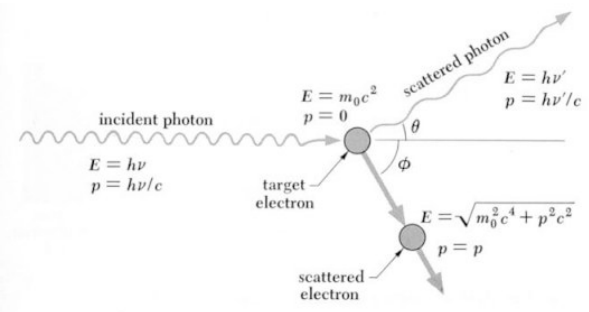


FIG. 1: Interaction picture of single photon Compton scattering (http://universe-review.ca/R15-12-QFT.htm#Compton).

$$\frac{\omega'}{\omega} = \frac{1}{1 + \frac{\hbar\omega}{m_e c^2}(1 - \cos\theta)}. \tag{1}$$

The Compton shift in the denominator is given by

$$\lambda = \frac{h}{m_e c} \sim 2.42 \times 10^{-24}\text{m}. \tag{2}$$

The probability that a photon will scatter into a certain direction is determined by summing over the possible permutations (*Feynman diagrams*) $M$ of a scattering process, thereby determining the cross section[2]. The Klein-Nishina cross section is calculated by summing over the transition probability amplitudes that our system in an initial state with momentum $P_i = p + k$ will scatter into a final state with momentum $P_f = p' + k'$. Accounting also for initial and final spin states $\mathbf{S}_i$ and $\mathbf{S}_f$, the cross section is function of the aforementioned 4-vectors and the probabilities amplitude and can be summed over the final energy-momentum space:

$$\begin{aligned}\sigma &= (2\pi)^2 \frac{\epsilon\omega}{|p_\mu k^\mu|}\mathbf{S}_f\mathbf{S}_i\delta(p' + k' - p - k)\,|\langle f|\,M\,|i\rangle|^2 \\ &= \left(\frac{e^2}{4\pi}\right)^2 \frac{1}{2\kappa\epsilon'\omega'}\int d^3p' d^3k' \delta(p' + k' - p - k)\,\bar{X}\end{aligned} \tag{3}$$

where $X$ is an *average* over all spin states, and $\epsilon = p^0$ and $\omega = k^0$ ($c = 1 = \hbar$ in natural units). Differentiation of this expression in the rest frame of the incident electron yields the polarization-dependent Klein-Nishina formula,

$$\frac{d\sigma}{d\Omega} = \frac{1}{4}r_0^2\left(\frac{\omega'}{\omega}\right)^2\left(\frac{\omega}{\omega'} + \frac{\omega'}{\omega} - 2 + 4|\hat{e}\cdot\hat{e}'|^2\right), \tag{4}$$

which can be averaged over all final polarization states to yield,

$$\frac{d\sigma}{d\Omega} = \frac{1}{2}r_0^2\left(\frac{\omega'}{\omega}\right)^2\left(\frac{\omega}{\omega'} + \frac{\omega'}{\omega} - \sin^2\theta\right), \tag{5}$$

where $r_0 = e^2/4\pi m$ is the classical electron radius. This cross section is anisotropic from its $\theta$-dependence and a

*Electronic address: mookerji@mit.edu, cherder@mit.edu

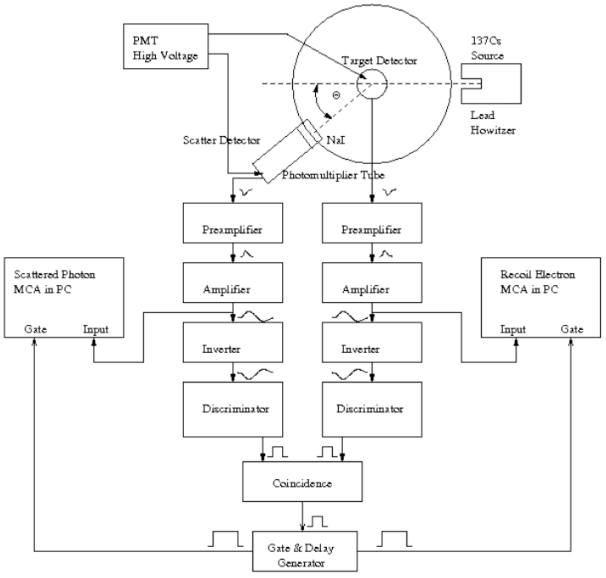


FIG. 2: Apparatus for Compton wavelength measurement. Decay events from a lead-encased 100mCi $^{137}$Cs source are scattered off of a fixed 2" × 2" Canberra Model 802-3/2007 (NaI) scintillator detector normal to the scattering plane. Compton scattered photons were measured as coincidences on a rotatable scintillator detector in the scattering plane of an approximately 20cm radius. [3].

function of the incident frequency of the electron, which may have a large relativistic kinetic energy compared to the rest mass of the electron. The classical elastic scattering, or Thompson, cross section can be recovered in the non-relativistic limit where $\omega' = \omega$. Integrating over solid angle $d\Omega$, the total electron cross-section is given by $0.2566\text{b}\left(1\text{barn} = 10^{-24}\text{cm}^2\right)$.

## 2. EXPERIMENTAL SETUP AND PROCEDURE

A schematic of our experimental apparatus and scattering arrangement is in Figure 2. Signals from the NaI scintillator are fed through a photomultiplier tube (PMT) biased at 1kV by a Canberra 3002D HV Power Supply and then discriminated into individual counts through a signal chain composed of a Canberra 805 scintillator preamplifier, a Ortec 533 Dual Sum and Invert Amplifier, and a Canberra 2126 Constant Fraction Discriminator. To eliminate background gamma ray events from the scatter detector, a coincidence detection scheme was used. An Ortec 418A Universal Coincidence required simultaneous signals ($\sim 1\mu$sec) from both detectors to occur before sending signals to the gate and delay generator. The gate and delay generator produced TTL pulses aligned with the amplifier output signal to the multichannel analyzer (MCA), largely eliminating background events in the scatter detector.

The spectrum on the MCA of each detector gave instance counts in each of 2048 bins divided by voltage.

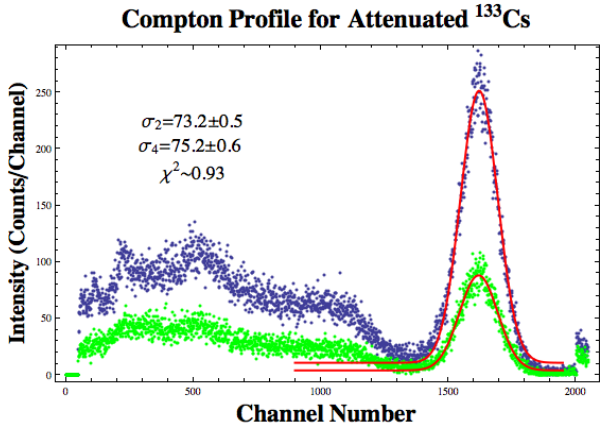


FIG. 3: Typical Compton profiles of photons scattered at 0° and attenuated by 2 and 4 blocks of polyvinyl toluene(PVT).

To measure the angular dependence of Compton scattering, we first perform a calibration relating the channel number of the MCA spectrum to the energy of known low-activity gamma ray sources $^{137}$Cs (661.6keV), $^{22}$Na (511keV), $^{133}$Ba (356, 302, and 81keV). The Compton energies are taken as the mean energies of Gaussian distributions fit to a region of interest using an LMA nonlinear-fitting algorithm in Mathematica 6. We vary the angle of the scatter detector and acquire coincidence measurements on the MCA, from which plotting functions of Compton energy and scattering angle yield the Compton wavelength, the associated electron mass, and the incident photon energy of the $^{137}$Cs source. The differential cross section of the process is determined by analytically integrating a given Gaussian fit for the total number of counts in the region of our fit.

To measure total cross section, we removed the target scintillator and coincidence detection and acquired MCA spectra of the 661.6keV $^{137}$Cs photopeak through varying thickness of polypropylene (PP), polyvinyl toluene (PVT), and polycarbonate (PC) in the immediate path of the source and the scatter scintillator at 0°. Integrated count rates were determined from Gaussian fits and plotted against target depth to determine an attenuation coefficient. Number density of electrons is determined from empirically by measuring the mass and dimensions of the blocks.

## 3. RESULTS AND ERROR ANALYSIS

Figure 2 depicts the a typical Compton photopeak found in our scattering experiment. We first discuss the errors contributing in quadrature to our determination of the Compton energies of scattered photons from these plots. We continue with a discussion quadrature counting errors contributing to our parameter error.

Photopeaks attributed to Compton scattering experience several broadening effects contributing to our error, and some negligible effects relevant to higher resolution

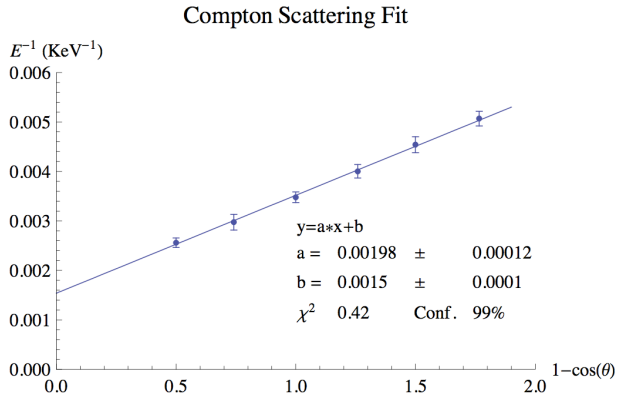


FIG. 4: Variation of photon energy with scattering angle.

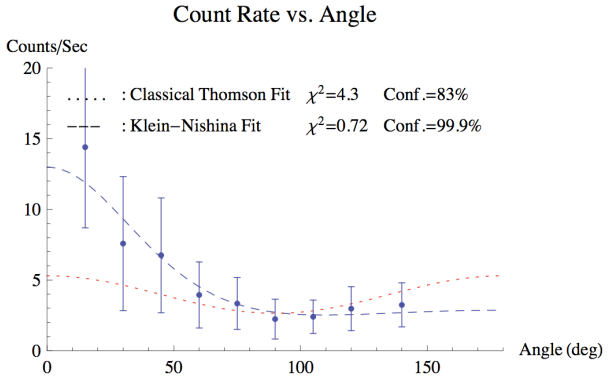


FIG. 5: Approximate Klein-Nishina differential cross section. The fits of the classical Thompson and Klein-Nishina differential cross sections indicate close agreement with the relativistic theory.

measurements. Inherent to our experimental setup is the spread of the beam profile ($\Delta\theta \sim 8°$) of the $^{137}$Cs source over the surface of the scatter detector that contributes to a Gaussian spread of measured scattering events. The Fermi motion of electrons in the detector has a finite momentum distribution contributing to Lorentzian line broadening beyond the resolution of the NaI scintillator[1]. Additionally, the motion of electrons about the binding potential of the nucleus Doppler broadens the apparent energy of incident photons from our source, thereby broadening the Compton peak for a given scattering angle. This contributes a relative error of less than 1% to the measured energy shifts [5].

Effects outside of broadening to error in our determination of Compton energies. The MCA spectrum of the Compton peaks are superimposed onto background noise and an exponentially decaying background from the Compton shelf. This error was minimized by fitting a Gaussian on top of a decaying exponential in the local region of interest. The statistical nature of a counting experiment added a standard Poisson error $\sqrt{n}/T$ for an acquisition time $T$.

Error in our cross section were propagated in quadrature as the $1\sigma$ error in the width and amplitude fit parameters of our Gaussians. Statistical error in the determination of the linear attenuation coefficient was taken as the $1\sigma$ error of the our nonlinear fitting in Mathematica.

### 3.1. Compton Wavelength

Figure 4 shows the variation of the center energies of these photopeak with a function of scattering angle, from which the Compton wavelength is determined and electron mass is determined to be $505 \pm 14$keV. The energy of the incident photon of the $^{137}$Cs gamma-ray source is measured to be $650 \pm 27$keV. Both are within within $1\sigma$ agreement of their respective published values $510.9889 \pm 0.00044$keV and $661.6 \pm 0.05$keV [1]. Furthermore, it was found that total energy of the scattered photon and scattered photon was constant within experimental error, but was consistently lower than the energy of the incident photon by approximately 30keV. This effect is attributed to energy loss in the NaI detectors themselves due to multi-step scattering in the PMT.

### 3.2. Klein-Nishina Cross Section

Our measurement of the Klein-Nishina differential cross section is in Figure 5. Here, the attenuation Compton events with angle is related to the cross section. The total number of photons $N'$ scattered through an angle $\theta$ into a solid angle $d\Omega$ in time $t$ is given by,

$$N'(\theta) = N n_e L t \left| \frac{d\sigma(\theta)}{d\Omega} \right| d\Omega \propto \frac{d\sigma(\theta)}{d\Omega}, \qquad (6)$$

where, $N$ is the number of incident photons per unit area per second, $n_e$ is the number density of scattering electrons, and $L$ is the length of the scatterer along the photon's path. The geometry here being fixed, the differential cross-section is directly proportional to the measured count rate at all angles. Figure 5 indicates that count rate as a measurement of cross section strongly favors the relativistic Klein-Nishina prediction.

The total cross section is determined from the dependence of linear attenuation of photons in a material with its number density of electrons. Aggregate data of count rate versus scattering depth is in Figure 6, and total cross section from number density of electrons is in Table I. The total number of scattering events is found by fitting a Gaussian profile to the background-subtracted spectra of a given material's Compton profile and then analytically

[1] Not surprisingly, the effect of Fermi motion can be easily determined for metals (e.g., Al foil) to which the free election gas model applies. Our setup would require a solid-state scintillator and a high-activity, low-energy gamma ray source (e.g., $^{241}$Am). See [4] for a more detailed discussion.

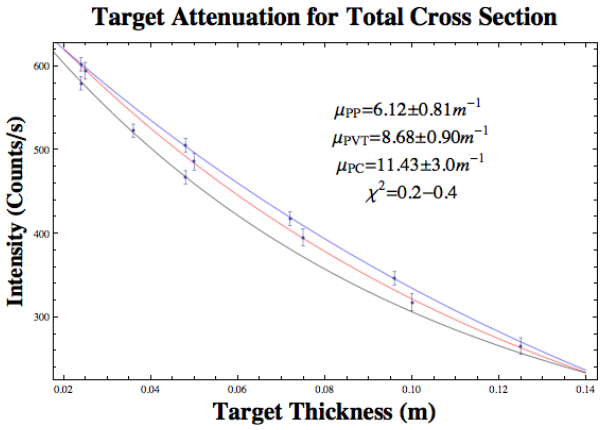


FIG. 6: Mass attenuation for polypropylene (PP), polyvinyl toluene (PVT), and polycarbonate (PC) (top down).

TABLE I: Total electron cross-section for polypropylene (PP), polyvinyl toluene (PVT), and polycarbonate (PC).

| Target | $\mu$ ($m^{-1}$) | $n_e$ ($10^{23}cm^{-3}$) | $\sigma$ (b) |
|---|---|---|---|
| PP $(C_3H_6)_n$ | $6.12 \pm 0.81$ | $3.03 \pm 0.04$ | $0.21 \pm 0.04$ |
| PVT $(C_{10}H_{11})_n$ | $8.68 \pm 0.90$ | $3.37 \pm 0.05$ | $0.25 \pm 0.03$ |
| PC $(C_{16}H_{14}O_3)_n$ | $11.43 \pm 3.00$ | $3.81 \pm 0.03$ | $0.28 \pm 0.04$ |
| Accepted | – | – | 0.26 |

integrating over its range using Mathematica 6. The linear attenuation coefficient $\mu$ for a material is determined by plotting counts in a fixed acquisition time against the total attenuation length of the material which has dependence on cross section $\sigma$ and density $\rho$ given by,

$$I(x) = I_0 e^{-\mu x} \qquad \mu = n_e \sigma = \rho \frac{NZ}{A} \sigma \tag{7}$$

where $N$ is Avogadro's Number, and $Z$ and $A$ are the electron and mass numbers respectively for a polymer unit it material. The cross section here is the sum of all cross sections from photon-matter interactions. Given our material (an insulating polymer) and our energy scales (661keV), we can conclude that photoelectric interactions in the target material and electron-positron production are negligible.

The exponential trend for PVT, PP, and PC in Figure 6 confirms that the change of intensity of the Compton profile $dI$ is proportional to the number density of electrons, and correspondingly the probability of Compton scattering occurrence governed by its cross section. This general trend of attenuation distance and number density of electron scattering centers is also found in Table I. Our determined electron cross-sections are within $1\sigma$ the accepted value.

## 4. DISCUSSION

In this experiment, we were confirmed several predictions of relativistic quantum mechanics in photon-electron interactions. We were unable to characterize some of complex geometric errors related to the finite detector size. Unfortunately, characterizing these errors is difficult measuring the beam profile and cross-section of the photon source. Also specifications were unavailable for the exact scattering geometry within the scintillator itself and the efficiency of the NaI crystal as a function of incident energy. A common assumption in this experiment is to assume that scattering takes place within the geometric center of the target scintillator (see Figure 2). The large finite size of our detectors (radius $R$) and detector separation radius $r$ implies that off-center geometric scattering may affect the measured value of scattering angle $\theta$. If we assume, for example, that a photon passes through the plane of the target scintillator and scatters at a radius $R$ from the center, the scattering angle of the target detector will instead be given by,

$$\cos\theta' = \frac{R\cos\theta - r}{\sqrt{R^2 + r^2 - 2rR\cos\theta}} \tag{8}$$

The including this corrections with the beam profile of the photon source will be an important correction for future instances of this lab.


[1] A. Melissinos, ed., *Experiments in Modern Physics* (Academic Press, 1996), chap. 1, pp. 95–104.
[2] J. Jauch and Rohrlick, *The Theory of Photons and Electrons* (Addisen-Wesley, 1955).
[3] S. Sewell, ed., *Junior Lab Reader* (8.13, 2007).
[4] K. H. S. Manninen and T. Paakari, Am. J. Phys. **56**, 928 (1988).
[5] F. Bloch, Phys. Rev. **46**, 674 (1934).